MARTENSIE PHASE TRANSFORMATION IN METASTABLE FULLY AUSTENITIC STEEL UNDER HIGH STRAIN RATE DEFORMATION

by

Ming Guan

A thesis submitted to Johns Hopkins University in conformity with the requirements for the degree of Master of Science in Engineering

Baltimore, Maryland
December 2020

Abstract

This essay discussed the influence of chemical composition, strain rate and grain size on martensite phase transformation in metastable fully austenitic stainless steel. Electron Back Scattering Microscopy (EBSD) was used to characterize the microstructure of samples and Split Hopkinson compression bar was applied to study the mechanical behavior of fully austenitic stainless steel under high strain rate deformation. The experiment results indicate that even tiny different Ni content can influence the stability of austenite under high strain rate deformation. Higher strain rate deformation makes the stainless steel's work-hardening larger low strain rate deformation. At last, small grain size can significantly increase the austenite phase's stability under high strain compression deformation. To further study the dynamic mechanical behaviors of metastable fully austenitic steel, Split Hopkinson tension bar is needed, and that is the major task for future work.

Primary Reader: Professor Todd Hufnagel

Table of Content

List of Tables

List of Figures

1. Introduction

Real life application often requires material to satisfy multiple criterions. For example, in a car crash accident, the frame of car made by high strength steel cannot guarantee the safety of passengers. The material must combine high strength and high ductility to absorb the crush energy to ensure the safety of driver and passengers. Another example is the material for cryogenic storage. Most material's ductility decreases under low temperature. Thus, the structural material for cryogenic storage must maintain high strength and ductility at low temperature environment. Although researchers are always looking for desirable materials combining high strength and high ductility, these two properties are contradictory. For instance, polymer based soft materials always have good ductility. They can be easily bend or stretched to multi self-length. However, they are also one of the weakest materials whose tensile stress are only several MPa or even KPa.

In recent decades, there are increasing interests focusing on transformation induced plasticity (TRIP) assisted steels due to their excellent combination of high strength and ductility [1,2]. This TRIP effect come from the strengthening mechanism named deformation-induced martensitic transformation (DIMT) which could prevent the strain localization to delay the fracture of material. With the application of TRIP effect and DIMT, significant progresses have been made in Advanced High Strength Steel (AHSS). Being different from traditional mild steel, AHSS like austenitic stainless steel, complex phase (CP), Ferritic-Bainitic (FB), twinning induced plasticity (TWIP) and duel phase (DP) steel exhibit unique high strength and uniform elongation length. The mechanical properties of traditional and advanced high strength steel are shown in the following diagram:

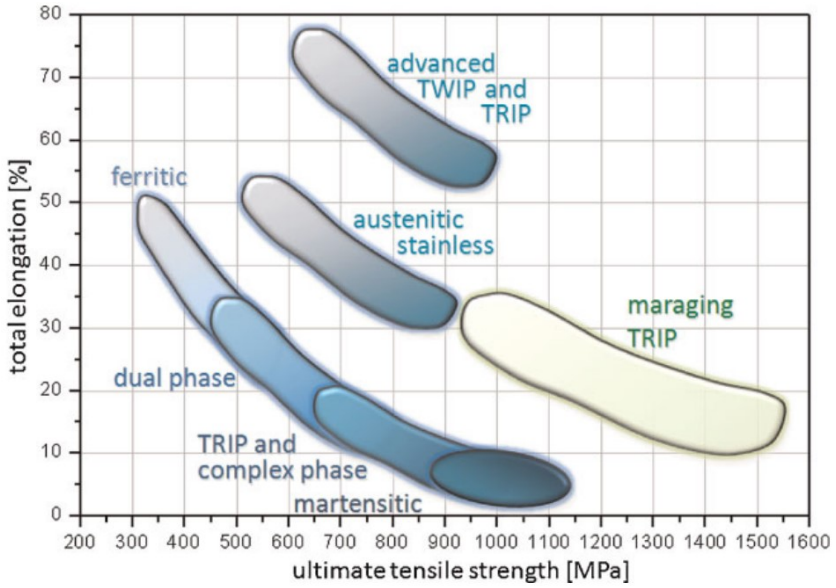

Figure 1: Tensile stress and Elongation of different steels [3]

The 3rd generation of AHSS exhibits ultra-high strength and maintains good ductility and has wide potential for manufacturing versatile structure materials at low costs. Their unique mechanical properties are achieved through microstructure tuning and special strengthening mechanisms. Most of these strengthening mechanisms have close relationship with phase transformation. In order to understand the details of phase transformation in steel materials, we need to know different phases in steel and their transformation mechanism.

1.1 Different phases of steel

The discussion on phase of steel will be focused on three different phases in this essay: Face-centered cube (FCC) austenite, Body-centered cubic (BCC) ferrite and Body-centered tetragonal (BCT) or sometimes BCC martensite. The Fe-C phase diagram explicates the transformation conditions for different phases and is shown below:

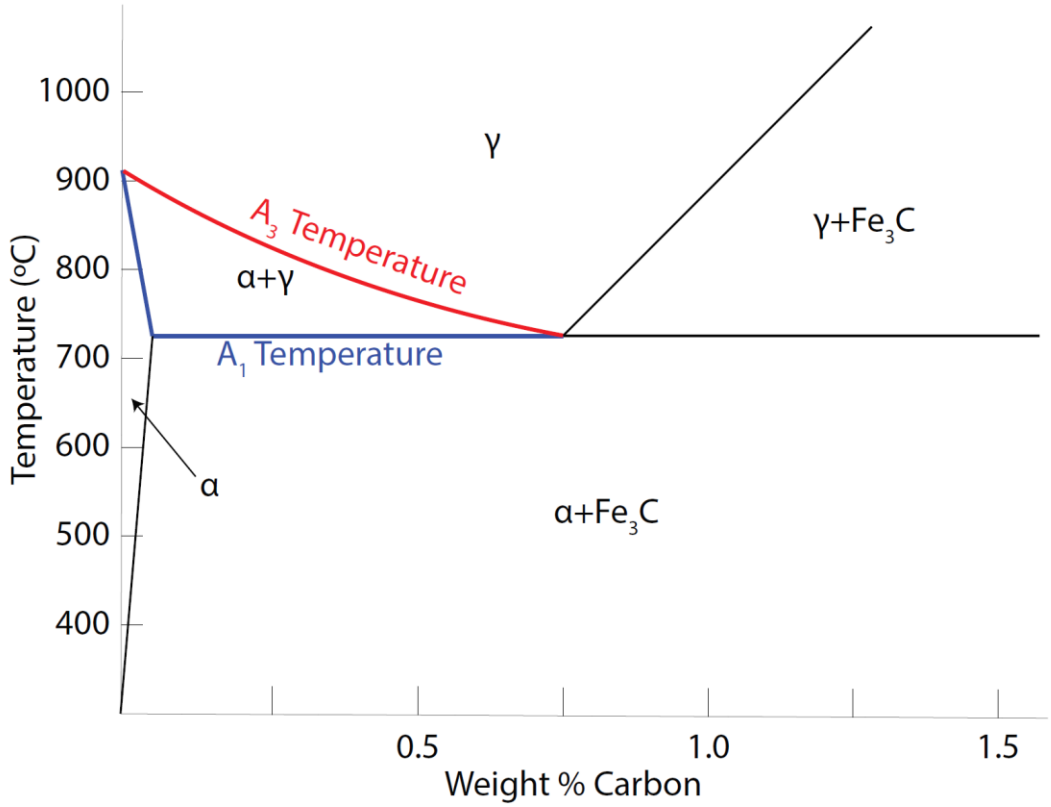

Figure 2: Fe-C binary phase diagram. (γ) stands for austenite and (α) stands for ferrite. [4]

At very high temperature, the austenite phase is the only stable structure in steel. When the temperature is below A_3, austenite is not the only stable phase. When the temperature keeps dropping down to below A_1, the austenite will transform to ferrite and cementite (Fe_3C). If the austenite phase is cooled down quickly (like quench) below martensite start temperature, the carbon atoms do not have enough time to diffuse out of austenite phase to form cementite. The austenite with remaining carbon will transform to martensite phase instead.

1.2 Martensite and martensite phase transformation

Martensite is a very hard phase of steel crystalline structure. When the austenite phase is quenched rapidly, the carbon atoms are trapped inside austenite phase, so the FCC structure austenite will instead transform to highly strained BCC or BCT crystalline structure called martensite. The martensite phase always has large amount of dislocations because of shear deformation. Although the word, martensite transformation, was initially created to describe the phase transformation of steels, the meaning of this word has been extended to many nonferrous alloys with the similar properties. For example, Titanium and related alloys also have "martensite phase transformation". The phase transformation process has been shown in the Figure 3:

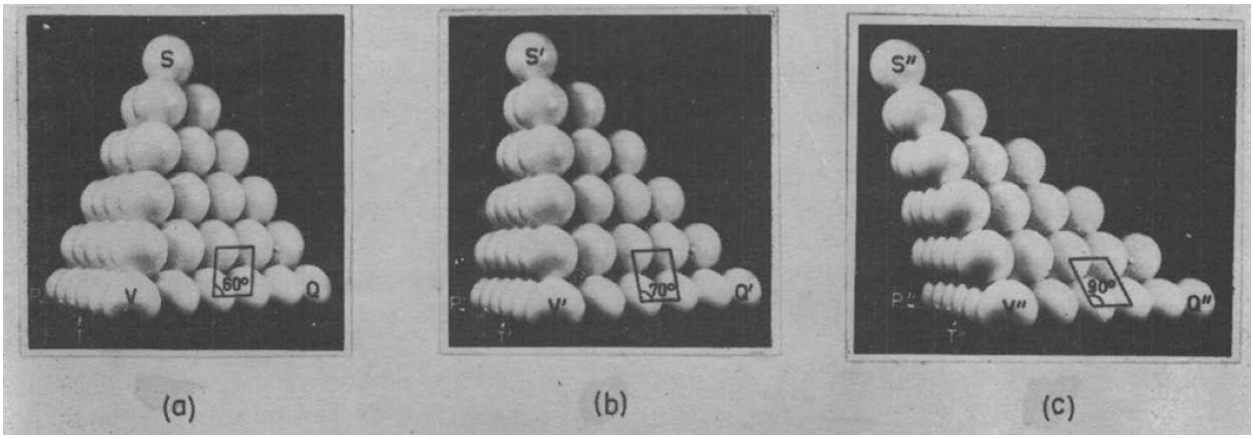

Figure 3: (a) Original tetrahedral arrangement of four {111> planes. (b) Intermediate status after 1/3 normal twin shear. The distance between successive {111} planes parallel to P'V'S' and P'V'Q' has increased by 5.4%. (c) Final position after complete twin shear. [5]

The BCT structure could be regarded as BCC lattice with the vertical axis elongated. That is the reason the symbol (') is used to distinguish martensite phase and ferrite phase. Figure 3(a) has shown the FCC packing of spheres in {111} planes. When the phase transformation begins, successive layers which are parallel to PVQ plane shear by (a/6) <112> in the direction of QT

which is perpendicular to PV. The whole shear process is divided to two steps: the first one is one-third of this shift, which is shown in Figure 3(b), while the final status is shown in Figure 3(c). The transformation process is also be presented in Figure 4:

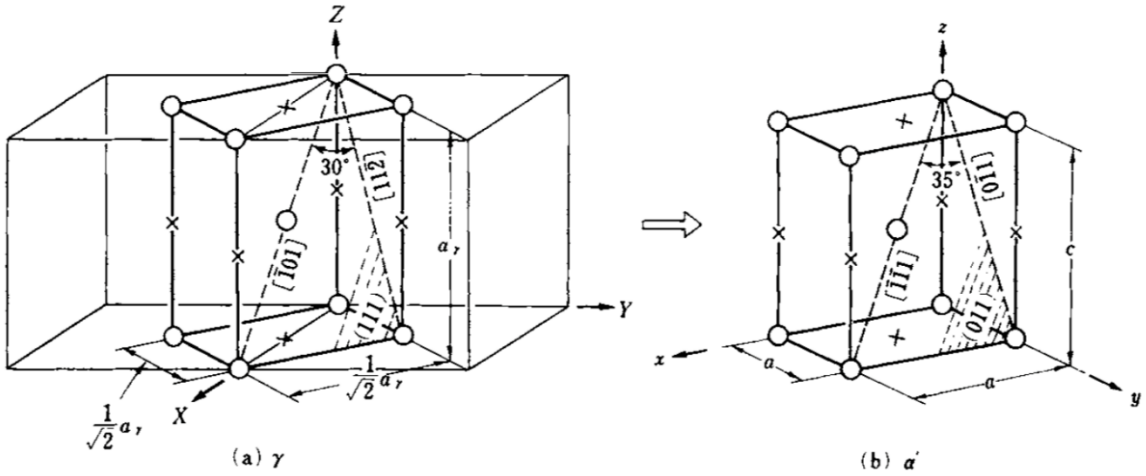

Figure 4: martensite transformation from (a) γ phase to (b) α' phase.[6]

Because of the close relationship between original austenite and the subsequent formed martensite, there is a definite orientation relation between these two phases. In carbon steels, the planes and orientations relationship are:

$$(111)_\gamma \parallel (011)_{\alpha'} \qquad [-101]_\gamma \parallel [-1-11]_{\alpha'}$$

This means the (111) plane of austenite phase is parallel to the (011) plane of new formed martensite phase, and the direction of original austenite phase [-101] is parallel to [-1-11] direction of martensite. These relationships are called Kurdjumov-Sachs (K-S) relations. In another system Fe-30%Ni alloys, this relationship has changed to Nishiyama relationship.

The most basic driving force for austenite to martensite phase transformation is chemical free energy. Because of different entropy, austenite and martensite's chemical energy change differently with the change of temperature. The relationship between temperature and the chemical energy difference is shown in Figure 5:

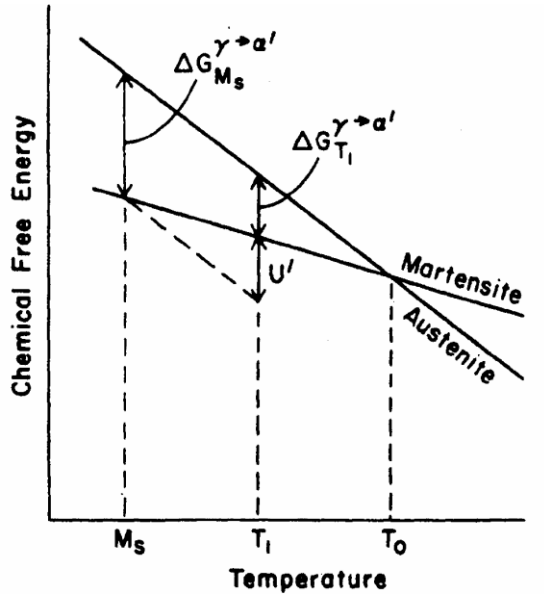

Figure 5: Relationship between chemical free energy and temperature.[7]

The slope of austenite is much steeper than martensite phase, so the chemical free energy of austenite is higher at low temperature range, so martensite phase is more stable than austenite at low temperature, while the austenite is a more stable phase at high temperature. The transition point of martensite phase transformation is called martensite start temperature (MS). However, this point isn't the balanced point of free energy of austenite and martensite. It is because of another form of energy, stacking fault energy (SFE), also influence the transformation process. The equation to express the stacking fault energy is shown below:

$$\gamma = n\rho_A(\Delta G^{chem} + E^{str}) + 2\sigma(n) \quad (1)$$

Stacking fault energy is γ, and n represents the thickness of atom layers. ρ_A stands for density of atoms and ΔG^{chem} is free chemical energy. E^{str} is strain energy and $\sigma(n)$ refers to free energy per unit area of interface. Although tradition research believed chemical free energy difference is the major driving force of phase transformation, recent study spotlights the important role of SFE. [8]

1.3 Factors influence martensite phase transformation

Based on the discussion on chemical driving force's effect on phase transformation, chemical component is one of the major factors that influence the transformation process. It is because different components directly decide different chemical free energy and stacking fault energy. For example, carbon and nickel are famous austenite phase stabilizers. Through changing the percentage of nickel, the stability of austenite can be modified. Nickel's percentage in steel is even more important when we synthesis fully austenitic stainless steel.

Except for chemical composition, temperature is another dominating factor in phase transformation. Austenite is always stable at high temperature and transform to martensite when the temperature drops down to martensite start temperature.

Grain size also influences the martensite phase transformation. It is accepted that smaller grain size crystal has greater resistance to martensite transformation [9]. The relationship between martensite start temperature and grain size has been shown below:

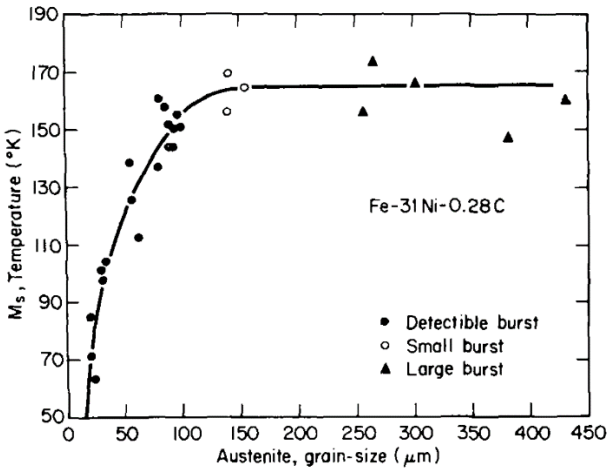

Figure 6: Relationship between austenite grain size and martensite start temperature.[9]

External force can also promote or prohibit the phase transformation process. This phenomenon is called deformation induced martensitic transformation (DIMT). The work has been down by external force acts the same as chemical driving force to promote the transformation. This conception has been further demonstrated by the fact that compression and tension force promote the phase transformation differently [10]. It is because the martensite phase transformation includes both shear displacement and dilatational displacement. The tension and compression force act the same on shear displacement while differently on dilatational displacement. The detailed relationship between stress and applied external force has been shown in Figure 7:

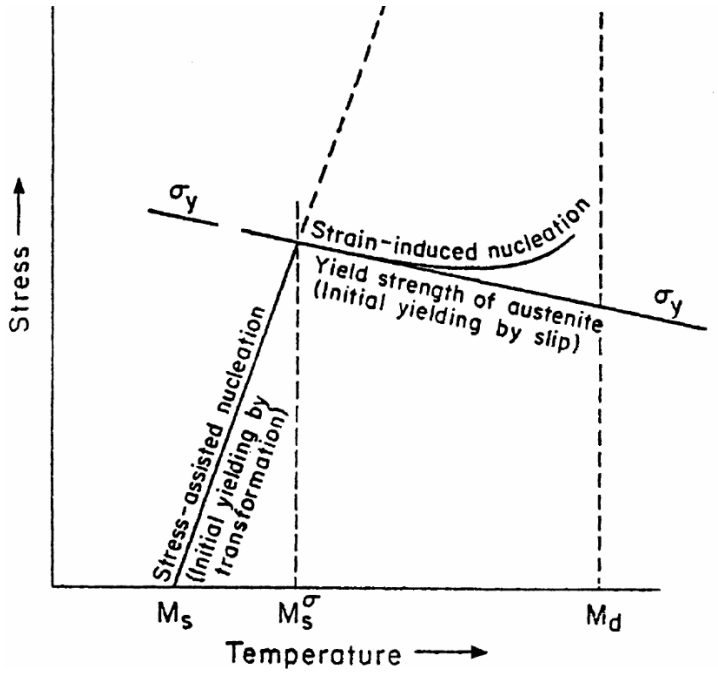

Figure 7: Critical stress to initiate martensitic transformation as a function of temperature.[11]

From Figure 7, it is clear that DIMT has two stages: stress-assisted and strain induced stage. The former one happens before the yield point of the material, and the stress to activate martensite phase transformation increase linearly with temperature. After the stress reaches yield stress of the material, strain replaces the stress to assist martensite phase transformation. The upper limit of this stage is the M_d temperature, above which martensite transformation no longer happens.

1.4 Nucleation sites and routes for martensite phase transformation

Just being the same as most phase transformation process, martensite phase transformation begins with the original nucleation sites. It has been demonstrated the intersection of shear bands or single shear band can be the nucleation site for strain induced martensite transformation while the grain boundary and grain boundary triple point are common nucleation sites for stress assisted martensite phase transformation.

There are two kinds of martensite phase with different crystalline structure. One is the previously discussed BCC martensite called α' martensite and the other one has HCP structure celled ε martensite. The transformation route is original γ phase transforms to ε martensite. ε martensite is one of the most importance sources of shear band. Then with the propagation of ε martensite, they will intersect with each other to form the final α' martensite. Although most of the martensite transformation happens in this way, there are still exceptions. Researchers also observed some original austenite directly transforms to α' martensite without intermediate steps [12]. Figure 8 has shown the formation of α' martensite in the intersection of shear bands.

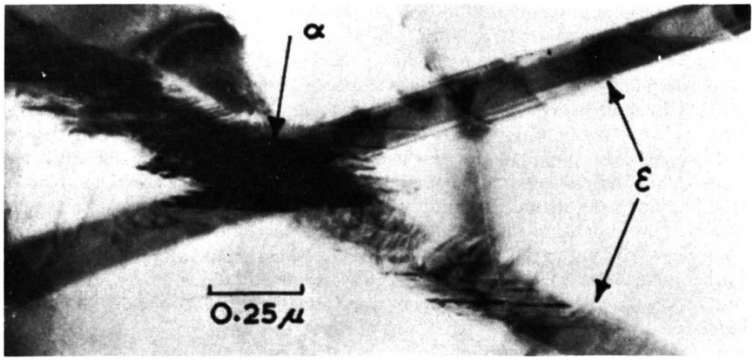

Figure 8: Nucleation of α' martensite [13]

1.5 Dynamic deformation technique

Quasi static tension test is the most common used mechanical test for steel material or even all metal materials. Most literatures adopted the results of quasi static tension test for mechanical property analysis. However, high strain rate deformation test is also of great importance. For example, as one of the most important application for TRIP steel, automobile application always undergoes high strain rate deformations. It has been demonstrated material has much different mechanical behaviors in dynamic loading condition than in quasi-static condition [14]. Therefore,

studying the mechanical properties of material under high strain rate deformation has great importance for our understanding of material's dynamic behaviors.

There are several methods to realize the high strain rate deformation of material. For example, laser shock experiment is one method to realize that purpose. The strain rate of that can reach 10^6 per second [15]. However, laser shock experiment cannot record the stress strain curve of the material. Besides, the sample will be damaged after the deformation. Sample recoverable experiment cannot be achieved by that method. Another commonly used method is Split-Hopkinson bar experiment. This method has unique advantages. Complete stress strain curve of the material can be recorded, and sample can be recovered after high strain rate deformation. All of these features make this method a powerful way to study the mechanical behaviors of material under dynamic loading.

Split Hopkinson bar is an apparatus which uses compressed gas to drive striker in order to realize high strain rate deformation under lab controllable condition. It can realize strain rate ranges from 10^3 to 10^4 per second. A schematic presentation of Split Hopkinson compression bar has been shown in Figure 9:

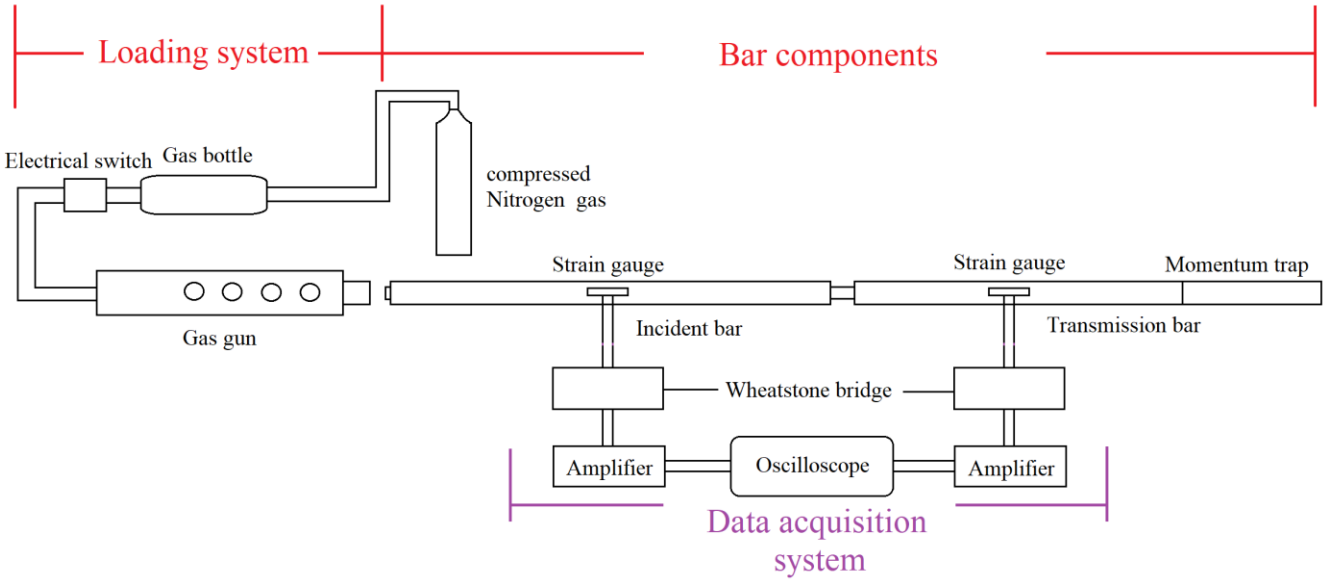

Figure 9: Schematic presentation of Split Hopkinson compression bar

Stress and strain information is recorded by strain gauges on both incident bar and transmission bar. To record these signals, a Wheatstone bridge consisted by two strain gauges and two resistors is applied. The diagram of Wheatstone bridge has been shown in Figure 10:

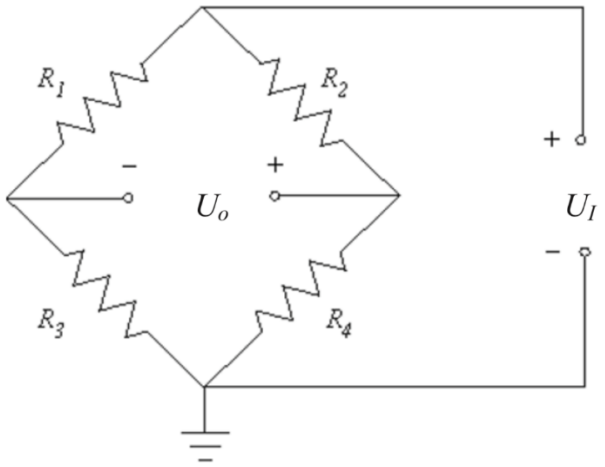

Figure 10: The Wheatstone bridge for Split Hopkinson bar system. [16]

In Figure 10, R1 and R4 are strain gauges while R2 and R4 are constant resistors. Equation (1.1) and (1.2) are used to calculate the strain of incident bar and transmission bar: [16]

$$U_0 = \frac{\frac{\Delta R}{R}}{2+\Delta R/R} U_I \approx \frac{1}{2}\frac{\Delta R}{R} U_I \tag{1.1}$$

$$G_F = \frac{\Delta R}{R}\frac{1}{\varepsilon} \tag{1.2}$$

U_I stands for the input voltage of the Wheatstone bridge. U_0 represents for the output voltage of Wheatstone bridge. G_F is the gauge factor and ε is the strain of incident bar or transmission bar. The stress of dynamic compression test is calculated by (1.3):

$$\sigma = \frac{1}{2}(\sigma_1 + \sigma_2) = \frac{1}{2} \cdot \frac{A_B}{A_s} \cdot E_B(\varepsilon_I + \varepsilon_R + \varepsilon_T) \tag{1.3}$$

The strain rate of sample is calculated by equation (1.4):

$$\varepsilon = \frac{v_1 - v_2}{L_s} = \frac{C_B}{L_s}(\varepsilon_I - \varepsilon_R - \varepsilon_T) \tag{1.4}$$

In the equation (1.3) and (1.4), A_B stands for the cross-section area of bars, and v1 and v2 represent for the speed incident bar and transmission bar. The detailed calculation process of stress and strain are represented and carefully discussed in the reference [16].

1.6 Sample preparation

To study the martensite phase transformation's influence on the mechanical property of fully austenitic steel, stainless steel samples with different chemical composition and grain size are needed to be prepared. Firstly, the raw high purity Fe (>99.95%), Ni (>99.9%) and Cr (>99.9%) have been melted by arc melting (The sample were melted 7 times at maximum power for 20 seconds each time). Although induction melting is another prevailing method to melt and mix metal elements, the induction melting apparatus we can access can only melt 15g sample one time. On the other hand, arc melting equipment in our lab can produce metal ingot with more than 50g mass. After

the mixing of different elements, samples were heated to 1200℃ for 24 hours at undergraduate lab to homogenize the sample. Although the sample has very close composition to 304 stainless steel and can resist corrosion, the sample cannot resist oxidation under high temperature. In order to protect the sample from serious oxidation, samples were sealed by vacuum glass tube. It has been shown in Figure 11:

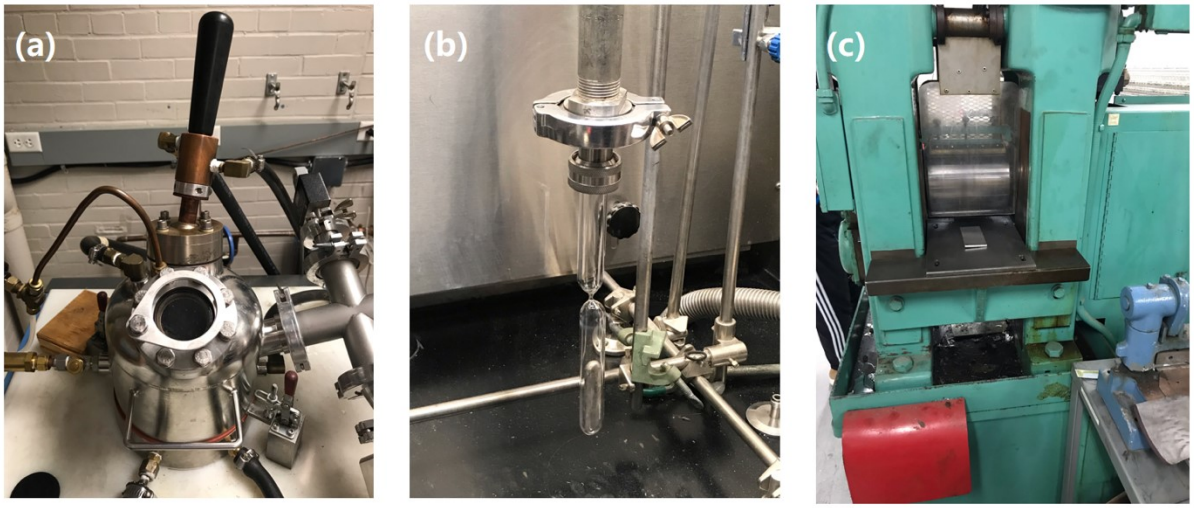

Figure 11: (a) arc melting equipment. (b) vacuum glass tube for sealing. (c) cold roller.

After homogenization, the samples were cold rolled to 80% thickness reduction at two times (each time 40% thickness reduction). Then samples were annealed at different temperature to synthesis fully austenitic steels with different grain sizes. The thermal history of fully austenitic steel samples has been shown in Figure 12. At last, annealed samples were cut by electrical discharge machining (EDM) to cube shape with 1 mm side length. Samples were also polished by electrical chemical polish for later microstructure characterization. Electrolyte is made by mixture of 10% perchloric acid and 90% acetic acid. The voltage is 36V and the current is 0.6A. The polished samples were prepared for Electron Back Scattering Diffraction (EBSD) characterization. For sample preparation of Split Hopkinson compression bar experiment, samples were polished

by polish paper (P1200) for 10 minutes at speed of 200 rpm, then polished by polish paper (P2500) for 30 minutes at 200 rpm, and finally by polish paper (P4000) for 30 minutes at 100 rpm.

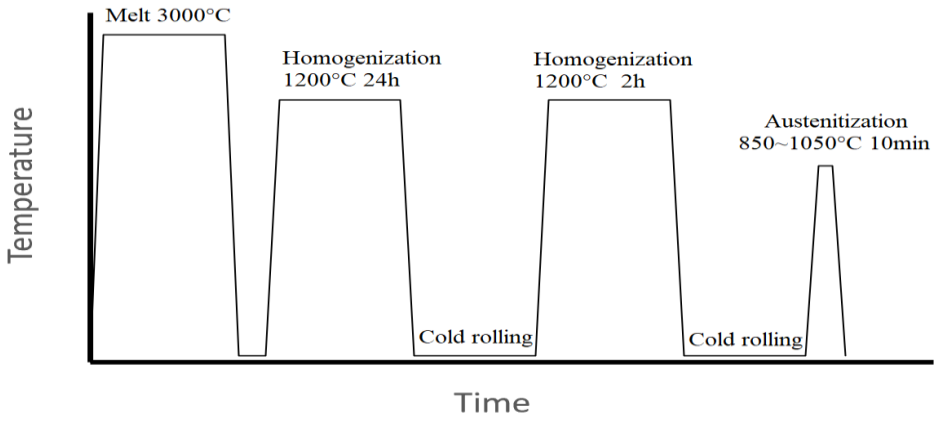

Figure 12: Thermal treatment history of fully austenitic steel samples

2. Result and discussion

2.1 Chemical composition influence on phase transformation

Four samples with different chemical compositions have been synthesized. In order to verify the repeatability of Split Hopkinson bar compression test in this essay, sample 1 and 2 were made in same conditions and same chemical compositions. It is the same for sample 3 and 4. More samples are tested are shown in Appendix A. The details of the samples have been shown on Table 1:

Sample	Chemical composition (wt %)	Anneal temperature	Anneal time	Average grain size (estimated by area average by EBSD software)
1	Fe-18Cr-10.2Ni	1050℃	11mins	45μm
2	Fe-18Cr-10.2Ni	1050℃	11mins	45μm
3	Fe-18Cr-11.0Ni	1050℃	11mins	45μm
4	Fe-18Cr-11.0Ni	1050℃	11mins	45μm

Table 1: Chemical compositions and annealing conditions for samples

After the samples were annealed, they were polished by polish machine (downstairs of Latrobe) by polish paper P1200, P2500, P4000 in turn and each turn for 20 minutes and 0 external force. After mechanical polish, the samples were polished by electrical chemical polish by mixture of 10% perchloric acid and 90% acetic acid. The voltage is 36V and the current is 0.6A. After that, samples were ready for EBSD characterization. The EBSD orientation mapping of samples has been shown in Figure 13:

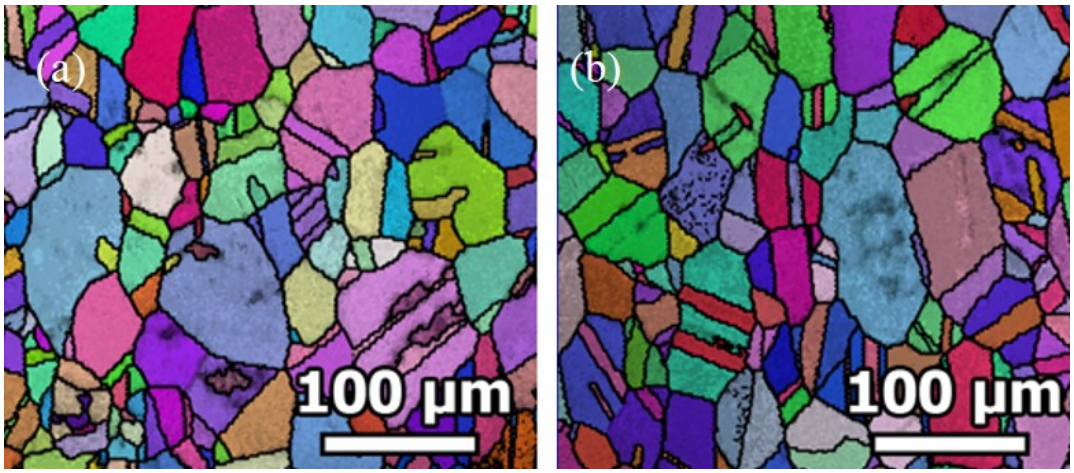

Figure 13: EBSD orientation mapping of samples. (a) Fe-18Cr-11.0Ni for 11 minutes annealing. (b) Fe-18Cr-10.2Ni for 11 minutes annealing.

It can be found in Figure 13 that almost all phases are austenite phase with annealing twinning. Martensite phase is negligible. The average grain size was calculated by software TEAM from EDAX by calculating area average.

These four samples have been deformed under 5000/s strain rate by Split Hopkinson compression bar system. Split Hopkinson compression bar system was used to collect the data. Incident bar was made by 17-4H hard stainless steel and 2 feet long, quarter inch diameter. Cupper pulse shaper with 2mm thickness was used. Striker is made by the same material as incident bar and was 1-foot-long quarter inch diameter. The loading direction is the normal direction of the samples.

The strain rate has been controlled through adapted suitable gas pressure and pulse shapers. Deformation strain rates for these four samples has been displayed in Figure 14:

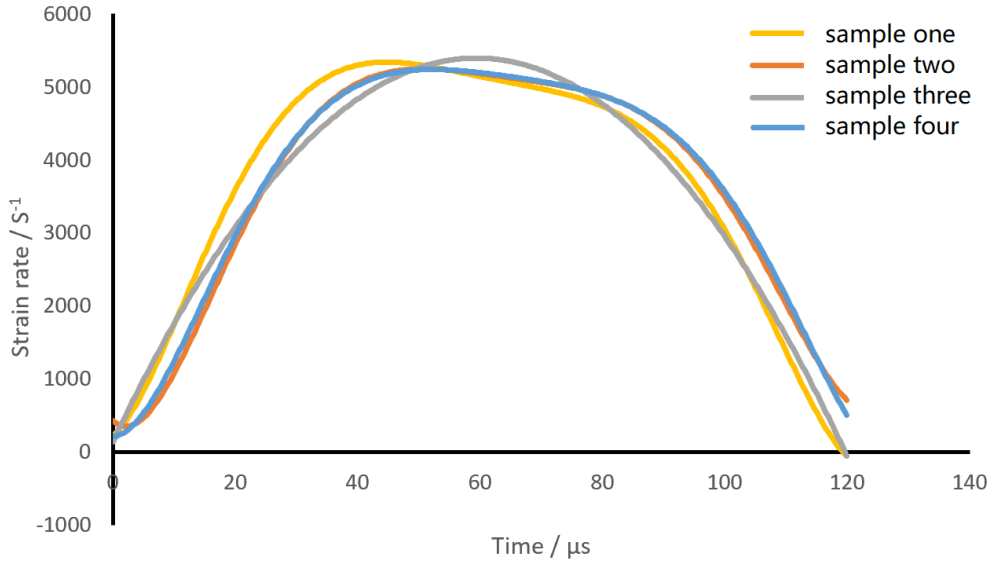

Figure 14: Compression strain rate of four samples

According to Figure 14, all four compression tests have very stable and repeatable deformation rates, which is the foundation for valid comparison among these high strain rate deformation tests. In another word, if the strain rate varies a lot in different high strain rate tests, the comparison between different high strain rate experiments is meaningless. The stress-strain curve of these four samples have been shown in Figure 15:

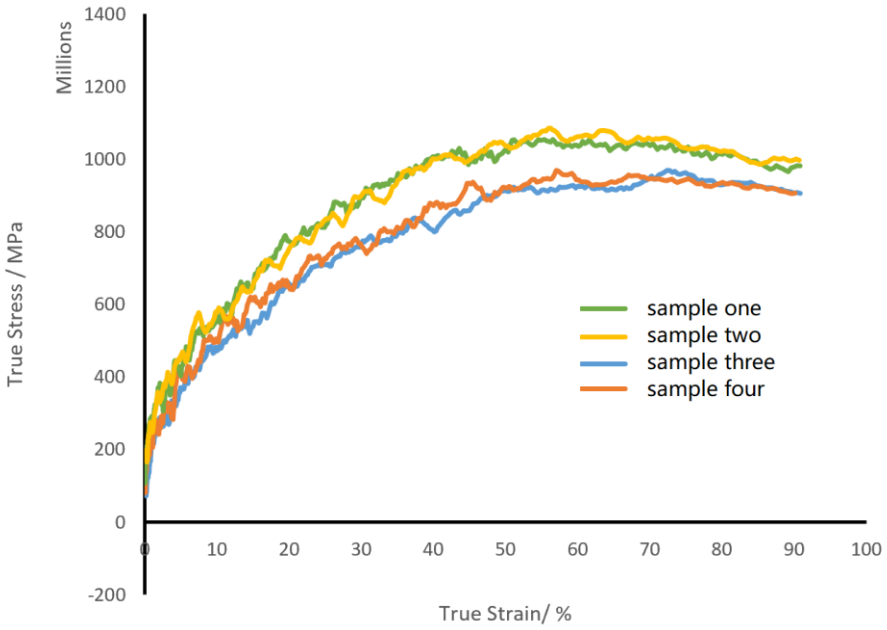

Figure 15: Stress-strain curve for four target samples

Figure 15, the fact that sample 1 and 2 almost overlap to each other indicates the good repeatability of the high strain rate deformation test. The similarity of stress-strain curves between sample three and four further demonstrates that. Fe-18Cr-10.2Ni samples (sample one and two) show higher work-hardening rate than Fe-18Cr-11Ni samples (sample three and four) because of the difference in chemical composition. It is widely accepted that Ni element works as the austenite stabilizer [17]. Higher Ni content can change the chemical driving force of martensite transformation in stainless steel material to change the stability of austenite. Fe-18Cr-10.2Ni has less Ni than Fe-18Cr-11Ni, so martensite phase transformation is easier to happen in Fe-18Cr-10.2Ni sample. It is possibly because martensite phase has high density of dislocation and is much harder than original austenite, the work-hardening rate of Fe-18Cr-10.2Ni is higher than Fe-18Cr-11Ni.

Another interesting phenomenon is that after 50% strain, the true stress of both Fe-18Cr-10.2Ni and Fe-18Cr-11Ni keep stable or even slightly drop down. Because true stress is reflecting

the real stress state of material, it generally keeps increasing before the fracture of material. However, the stress-strain curves of both materials slightly drop after 50% strain. This phenomenon is possibly caused by thermal softening effect. Different from quasi-static test, high strain rate deformation experiments generally use less than 100 μs, which is too fast for heat to dissipate. Sample will be heated up by tens of Celsius because of the work which has been done by external load [18]. This situation gets even more significant when strain is large. High temperature makes the dislocation much easier to move to decrease the flow stress of material. That is one explanation for the decreasing of true stress in Fe-18Cr-10.2Ni and Fe-18Cr-11Ni under high strain rate deformation. The material keeps room temperature during the whole deformation process. Considering the only difference between two deformation tests (quasi-static and high strain rate) is the strain rate, it is high possible the thermal softening effect contributes to the uncommon drop of true stress in high strain rate condition. Furthermore, the decreasing tendency of Fe-18Cr-10.2Ni is larger than that of Fe-18Cr-11Ni according to Figure 15. This is because the flow stress of Fe-18Cr-10.2Ni is larger than that of Fe-18Cr-11Ni. The work has been done by force is calculated by W=F×S, where F stands for force and S stands for distance. The applied force on Fe-18Cr-10.2Ni is larger than that of Fe-18Cr-11Ni, so the heat accumulated in Fe-18Cr-10.2Ni sample is also larger than of Fe-18Cr-11Ni sample. Thus, the Fe-18Cr-10.2Ni sample should have higher temperature than Fe-18Cr-11Ni sample. The higher temperature in Fe-18Cr-10.2Ni possibly explains the difference of true stress in high strain region between Fe-18Cr-10.2Ni and Fe-18Cr-11Ni.

2.2 The influence of strain rate on martensite phase transformation

Strain rate's influence on martensite phase transformation is always an interesting topic for industry field. It is because real-life applications always require material have acceptable performance

under both quasi-static and high strain rate deformation. To study strain rate's influence on martensite transformation, two samples with the same chemical composition and grain size have been prepared. Both samples have composition of Fe-18Cr-10.2Ni and average grain size of 45 μm. They were compressed under different strain rates to study their dynamic mechanical behaviors. The stress-strain curves of both samples are shown in Figure 16:

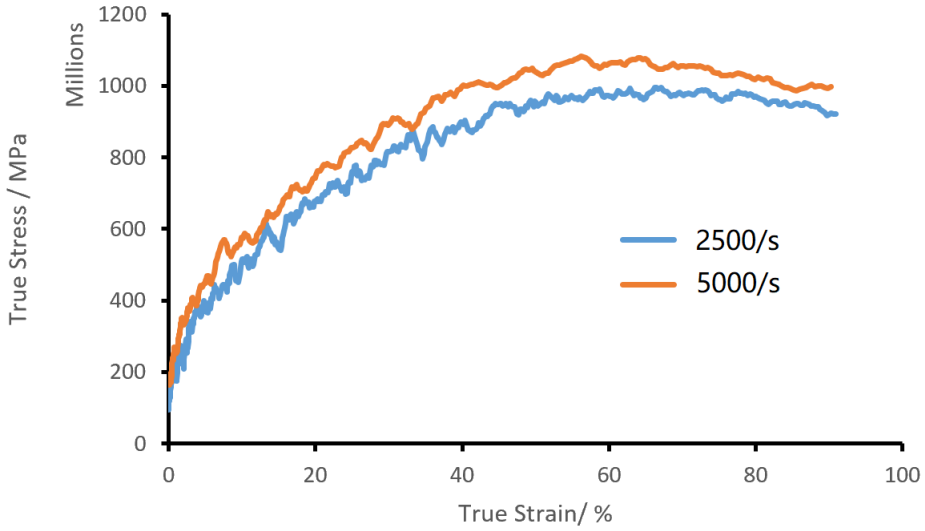

Figure 16: Stress-strain curve for Fe-18Cr-10.2Ni samples

High Strain rates influence martensite phase transformation in multiple ways. First, high strain rates leave little time for heat to dissipate, so the local temperature of sample increases under high strain rates deformation. Because austenite is a more stable phase than martensite when temperature is high, high temperature promotes the stability of austenite. Thus, sample under higher strain rate suffers more from thermal softening effect as we discussed previously. However, in Figure 16, the sample under higher strain rate deformation exhibits higher work-hardening rate, which indicate the phase transformation of austenite to martensite is faster in that sample. This result contradicts to the previous analysis that high strain rate will generate more heat to limit the martensite phase transformation. It is because strain rates influence phase transformation in more

than one way. Except for thermal softening effect, high strain rate also makes the movement of dislocation much harder than quasi-static deformation. For example, dislocations may pile up on the grain boundary rather than glide across the boundary in high strain rate condition. Furthermore, it has been demonstrated that high strain rate promotes the formation of nucleation sites for martensite transformation [19]. These factors overthrow the influence of thermal softening effect. That explains the higher work-hardening rate and flow stress in high strain rate condition.

2.3 The influence of grain size on martensite phase transformation

Grain size's influence on martensite phase transformation has been demonstrated before [20]. Smaller grain trends to have lower martensite start temperature. In the range from 1 micron to hundreds of microns, it is always true that smaller grain has higher austenite stability. In order to study grain size's effect on fully austenitic stainless steel under high strain rate deformation, two samples with the same chemical composition but different grain size have been made. The details of samples used in this section has been shown as the following Table:

Sample	Chemical composition	Annealing temperature	Annealing time	Average grain size (estimated by area average by EBSD software)
FASS-1	Fe-18Cr-	1050℃	5 mins	35 μm
FASS-2	Fe-18Cr-	850℃	5 mins	5 μm

Table 2: Chemical compositions and annealing conditions for samples

Sample FASS-1 (fully austenitic stainless steel) and FASS-2 have been polished through electrochemical polishing for EBSD characterization. The EBSD image of sample have been shown in Figure 17:

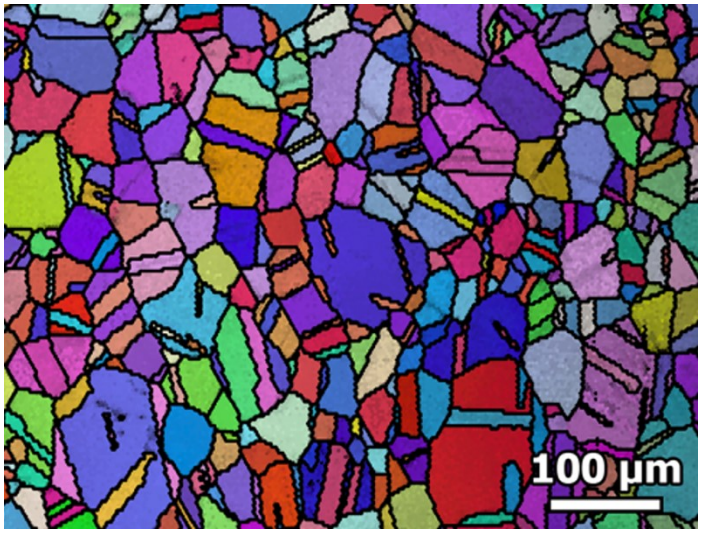

Figure 17: EBSD image of sample FASS-1

Because of the chemical polish machine has been down for more than three months and even the ion mill was down, I couldn't collect SEM image for FASS-2. However, I found one literature adopted very close chemical composition as FASS-2. These samples in that paper adopted a very similar cold-rolling then annealing process as this essay. The relationship between annealing time and grain size has been shown in Figure 18:

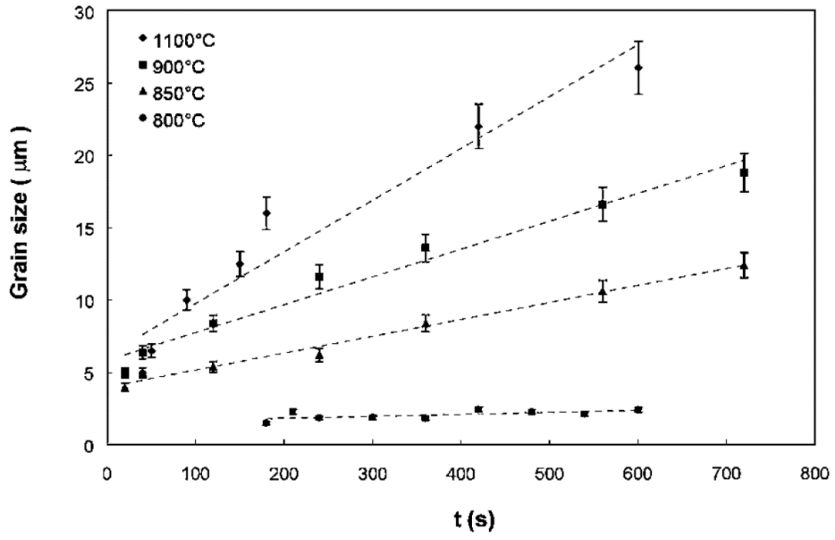

Figure 18: Grain size and annealing time relationship for Fe-18Cr-9Ni [21]

According to Figure 18, I speculated the grain size of FASS-2 is 5 μm.

Different grain size of these two samples were achieved by changing the annealing temperature. According to kinetic theory, the nucleation and growth of new phase need energy. Although chemical driving force is the fundamental driving force of phase transformation, the reaction rate highly depends on temperature. When temperature is high, the migration of atoms is much faster than in low temperature, so high temperature can accelerate the growth of martensite nuclei. Although low temperature has many advantages in making small size grain in fully austenitic stainless steel, it can not be lower than A3 temperature. This has been discussed in introduction section. Only above that temperature, the martensite phase transformation can happen. After annealing and polishing, these two samples were compressed under high strain rate (5000/s) by Split Hopkinson compression bar to characterize their mechanical properties. The stress-strain curve of these two samples has been shown below:

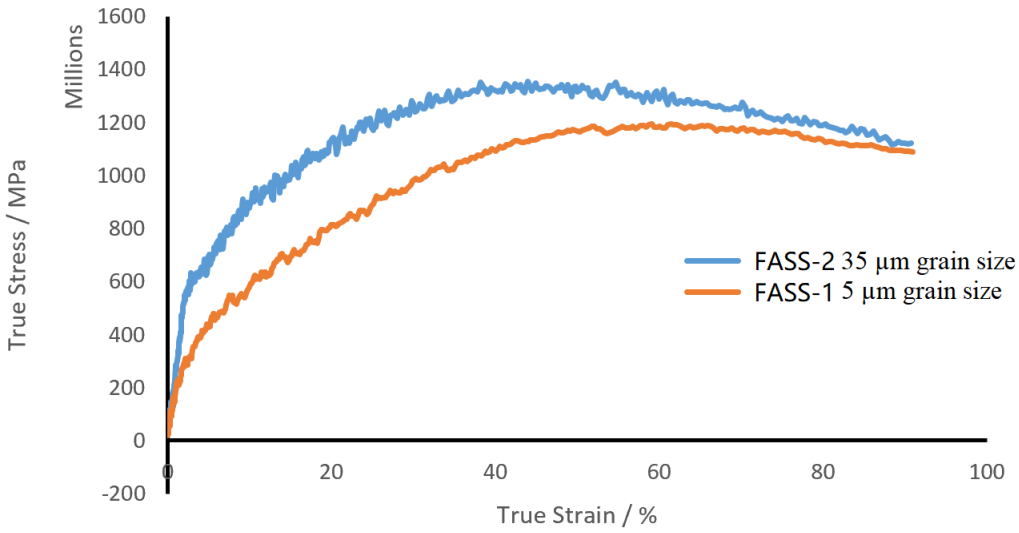

Figure 19: Stress-strain curve for FASS-1 and FASS-2

Although it is widely accepted that smaller grain is more stable than larger grain, the stress-strain curves of FASS-1 and FASS-2 indicate this statement is not always true. At small strain

range (0% to 10%), the work-hardening rate of small grain sample is actually greater than that of large grain size sample, although after 25% strain the work-hardening rate of large grain size sample is faster, which corresponds with grain size's influence on martensite phase transformation in previous study. The fast work-hardening rate of smaller size sample is because of the existence of remaining martensite phase in the sample. Because FASS-2 adopted low annealing temperature 850 Celsius, which is very close to inter-critical annealing temperature, this choice resulted in the existence of remaining martensite phase in the sample. It is possible that these small martensite phases provide nuclei for martensite phase transformation. It is widely accepted in kinetic theory that phase transformation needs to overcome the energy barrier of critical nucleation size. Only nuclei with larger size than critical nucleation grain size can stably grow to large grain, so the formation of stable nuclei is difficult for phase transformation even when the chemical driving force is existing. The remaining martensite can assist the martensite phase transformation by acting as the nucleation site for phase transformation. New martensite phase can grow directly on the pre-existing martensite nuclei rather than wasting energy on overcoming the energy barrier for the formation of nuclei bigger than critical nucleation grain size.

The flow stress of FASS-2 is always larger than that of FASS-1 because FASS-2's grain size is smaller. This corresponds to traditional theory that material with small grain size trends to have higher flow stress [22]. For FASS-1, the true stress starts to decrease after 65%, while the true stress of FASS-2 starts to decrease after 40% strain. The reason for the decreasing of true stress has been discussed in previous section. The true stress of FASS-2 starts to decrease earlier than FASS-1 because of its high flow stress. Because $W=F\times S$, larger applied force makes the strain smaller for the same amount of heat. That explained why the true stress of FASS-2 drops earlier than FASS-1.

2.4 Dynamic tension test for stainless steel

Up to now, we have tried two different Split Hopkinson tension bars to test stainless steel's tension properties under high strain rate tension deformation. The first bar system we used Justin Roe's tension bar, which has been discussed in Justin's master essay. The second design has been shown in detail at Appendix B. However, both Split Hopkinson tension bar cannot record reliable stress and strain information of material. The biggest problem is the stress signal of transmission bar. The stress signal of transmission bar, which is shown in Figure 20(a), was absurd. It is unlikely to abstract valid information from that signal. Then we figured out the pin-hole structure at the bar head, which was used to grip the sample to bars, caused this absurd signal. After adding adhesive in the hole of bar head to stick the position pin and sample to the bar, the stress signal has been significantly improved as Figure 20(b).

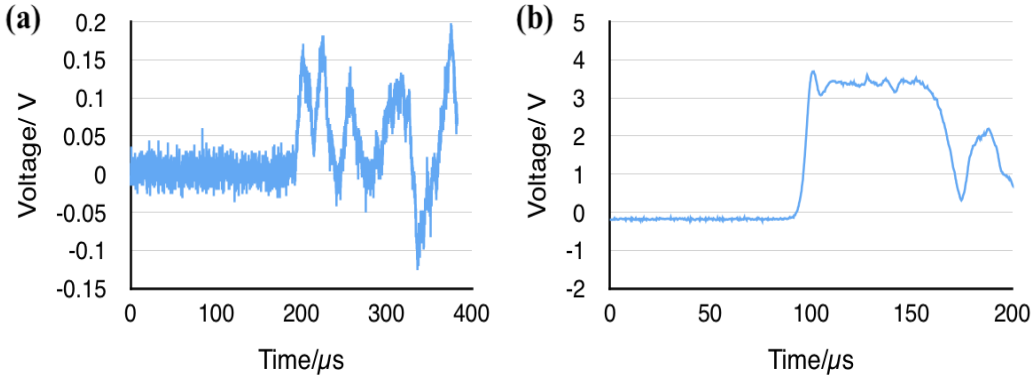

Figure 20: (a) Stress signal from strain gauge on transmitted bar during tensile deformation. (b) Stress signal from strain gauge on transmitted bar after added adhesive.

However, due to the numerous amounts of samples we need to test in a short time at DCS, we cannot rely on using adhesive to grip the position pin and samples. Better design is still needed for a successful tension test.

3. Conclusion and future suggestion

This work synthesized fully austenitic stainless steel samples and examined the factors that influence martensite phase transformation in these materials under high strain rate deformation. Based on the collected data, these conclusions have been drawn: (1) stainless steel with less Ni content has poor austenite stability and is easier to transform to martensite phase under high strain rate compression. (2) The martensite phase transformation is faster under higher strain rate deformation at small strain range (smaller than 40%). At high strain, the sample's mechanical behavior is strongly influenced by the heat produced by deformation at high strain rate. (3) Small grain size sample generally exhibits more austenite stability than large grain size sample. However, at small strain, the retained martensite influences the stability of small grain and the martensite phase transformation may be even faster in small grain.

Although high strain rate compression test has been applied to fully austenitic stainless steel samples, the tension test data is absent. It is because we cannot record repeatable and reliable tension test data up to now. Currently used Split Hopkinson tension bar in our lab has difficulty in recording reliable transmission bar data or even incident bar data. Keep refining current tension bar has little meaning, so a new design for Split Hopkinson tension bar is urgently need for study on fully austenitic stainless steel. Besides, the most used mechanical test on steel material is tension test rather than compression test, so develop a reliable Split Hopkinson tension bar is of great importance for study on martensite phase transformation in fully austenitic steels. However, the design and theory on Split Hopkinson tension bar is far more difficult than compression bar, especially for small size sample which has the potential to be used as study material in synchrotron-based X-ray diffraction experiment.

High strain rate deformation experiment which is characterized by synchrotron-based X-ray diffraction is a powerful tool to *in-situ* study the phase transformation in TRIP steel or other materials. One of the biggest disadvantages of current high strain rate deformation experiment is that all characterizations are *ex-situ*, which cannot obverse many transit states of material. For example, if the phase transformation rate is not constant, or there are some other intermediate phases have been formed during the deformation process but vanish at the end of deformation, current method cannot identify them. However, these non-uniform phase transformation and transit phase are critical for the study on martensite phase transformation. We had a planned *in-situ* high strain rate compression deformation experiment at Advanced Photon Source (APS) in April 2020, but it has been cancelled due to COVID-19 pandemic.

The *in-situ* high strain rate deformation experiment in multi stress states is one of future directions in martensite phase transformation study and other phase transformation study.

4. Acknowledgement

Thank Prof. Todd Hufnagel, Dr. Tian Ye, Dr. Minju Kang, Dr. Andrew Loeng, Sheng Hao, Jackson Wu for all the help. Funding for this work was provided by the Department of the Navy, Office of Naval Research under ONR award N000141812604. Any opinions, findings, and conclusions or recommendations expressed in this material are those of the author and do not necessarily reflect the views of the Office of Naval Research.

Reference

1. B.B. He, H.W. Luo, M.X. Huang, Experimental investigation on a novel medium Mn steel com bining transformation-induced plasticity and twinning-induced plasticity effects, Int. J. Plast. 78 (2016) 173–186. doi: 10.1016/j.ijplas.2015.11.004.

2. Z. Li, C.C. Tasan, K.G. Pradeep, D. Raabe, A TRIP-assisted dual-phase high-entropy alloy: Grain size and phase fraction effects on deformation behavior, Acta Mater. 131 (2017) 323–335. doi: 10.1016/j.actamat.2017.03.069.

3. Bieler, T. R., et al. "The role of heterogeneous deformation on damage nucleation at grain boundaries in single phase metals." International Journal of Plasticity 25.9 (2009): 1655-1683.

4. P.K. Lambert, Characterizing the martensitic transformation in a 10% nickel steel during dynamic deformation using *in situ* x-ray diffraction. PhD dissertation of Johns Hopkins University, 2017.

5. Olson, G. B., and Morris Cohen. "A mechanism for the strain-induced nucleation of martensitic transformations." Journal of the Less Common Metals 28.1 (1972): 107-118.

6. Nishiyama, Zenji. Martensitic transformation. Elsevier, 2012.

7. J. Talonen, H. Hänninen, Formation of shear bands and strain-induced martensite during plastic deformation of metastable austenitic stainless steels, Acta Mater. 55 (2007) 6108–6118. doi: 10.1016/j.actamat.2007.07.015.

8. J. Talonen, H. Hänninen, Formation of shear bands and strain-induced martensite during plastic deformation of metastable austenitic stainless steels, Acta Mater. 55 (2007) 6108–6118. doi: 10.1016/j.actamat.2007.07.015.

9. Umemoto, M., and W. S. Owen. "Effects of austenitizing temperature and austenite grain size on the formation of athermal martensite in an iron-nickel and an iron-nickel-carbon alloy." Metallurgical transactions 5.9 (1974): 2041-2046.

10. Patel, J. R., and Morris Cohen. "Criterion for the action of applied stress in the martensitic transformation." Acta metallurgica 1.5 (1953): 531-538.

11. J. Talonen, H. Hänninen, Formation of shear bands and strain-induced martensite during plastic deformation of metastable austenitic stainless steels, Acta Mater. 55 (2007) 6108–6118. doi: 10.1016/j.actamat.2007.07.015.

12. Das, Arpan, et al. "Morphologies and characteristics of deformation induced martensite during tensile deformation of 304 LN stainless steel." Materials Science and Engineering: A 486.1-2 (2008): 283-286.

13. Olson, G. B., and Morris Cohen. "A mechanism for the strain-induced nucleation of martensitic transformations." Journal of the Less Common Metals 28.1 (1972): 107-118.

14. Hecker, S. S., et al. "Effects of strain state and strain rate on deformation-induced transformation in 304 stainless steel: Part I. Magnetic measurements and mechanical behavior." Metallurgical Transactions A 13.4 (1982): 619-626.

15. Zhang, Wenwu, Y. Lawrence Yao, and I. C. Noyan. "Microscale laser shock peening of thin films, part 1: Experiment, modeling and simulation." J. Manuf. Sci. Eng. 126.1 (2004): 10-17.

16. Chen, Weinong W., and Bo Song. Split Hopkinson (Kolsky) bar: design, testing and applications. Springer Science & Business Media, 2010.

17. R.D.K. Misra, V.S.A. Challa, P.K.C. Venkatsurya, Y.F. Shen, M.C. Somani, L.P. Karjalainen, Interplay between grain structure, deformation mechanisms and austenite stability in phase-reversion-induced nanograined/ultrafine-grained austenitic ferrous alloy, Acta Mater. 84 (2015) 339–348. doi:10.1016/j.actamat.2014.10.038.

18. Hecker, S. S., et al. "Effects of strain state and strain rate on deformation-induced transformation in 304 stainless steel: Part I. Magnetic measurements and mechanical behavior." Metallurgical Transactions A 13.4 (1982): 619-626.

19. Umemoto, M., and W. S. Owen. "Effects of austenitizing temperature and austenite grain size on the formation of athermal martensite in an iron-nickel and an iron-nickel-carbon alloy." Metallurgical transactions 5.9 (1974): 2041-2046.

20. Hecker, S. S., et al. "Effects of strain state and strain rate on deformation-induced transformation in 304 stainless steel: Part I. Magnetic measurements and mechanical behavior." Metallurgical Transactions A 13.4 (1982): 619-626.

21. Jiang, Maoyuan, Benoit Devincre, and Ghiath Monnet. "Effects of the grain size and shape on the flow stress: A dislocation dynamics study." International Journal of Plasticity 113 (2019): 111-124.

22. Schino, A. DI, I. Salvatori, and J. M. Kenny. "Effects of martensite formation and austenite reversion on grain refining of AISI 304 stainless steel." Journal of Materials Science 37.21 (2002): 4561-4565.

Appendix A Sample lists

sample	Chemical composition (wt%)	Annealing temperature	Anneal time	Strain rate
1	Fe-18Cr-10.2Ni	1050℃	5 mins	2500/s
2	Fe-18Cr-10.2Ni	1050℃	11mins	5000/s
3	Fe-18Cr-10.5Ni	1050℃	5 mins	2500/s
4	Fe-18Cr-10.5Ni	1050℃	11mins	5000/s
5	Fe-18Cr-11Ni	1050℃	5 mins	2500/s
6	Fe-18Cr-11Ni	1050℃	11mins	5000/s
7	Fe-18Cr-10.2Ni	1050℃	5 mins	2500/s
8	Fe-18Cr-10.2Ni	1050℃	11mins	5000/s
9	Fe-18Cr-10.5Ni	1050℃	5 mins	2500/s
10	Fe-18Cr-10.5Ni	1050℃	11mins	5000/s
11	Fe-18Cr-11Ni	1050℃	5 mins	2500/s
12	Fe-18Cr-11Ni	1050℃	11mins	5000/s
13	Fe-18Cr-10.2Ni	850℃	5 mins	2500/s
14	Fe-18Cr-10.2Ni	850℃	5 mins	5000/s
15	Fe-18Cr-10.5Ni	850℃	5 mins	2500/s

16	Fe-18Cr-10.5Ni	850℃	5 mins	5000/s
17	Fe-18Cr-11Ni	850℃	5 mins	2500/s
18	Fe-18Cr-11Ni	850℃	5 mins	5000/s

Appendix B Design for Split Hopkinson Tension Bar

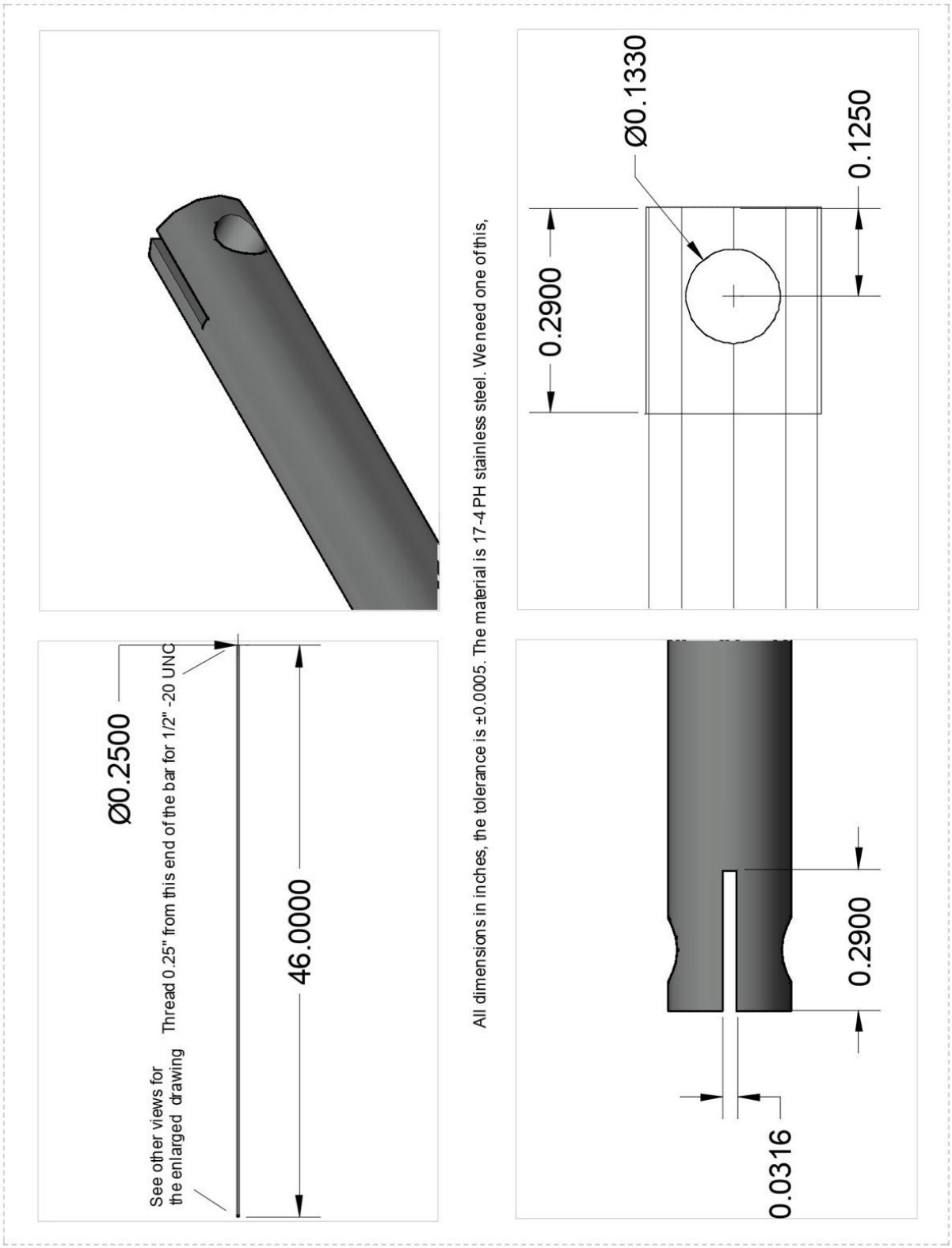

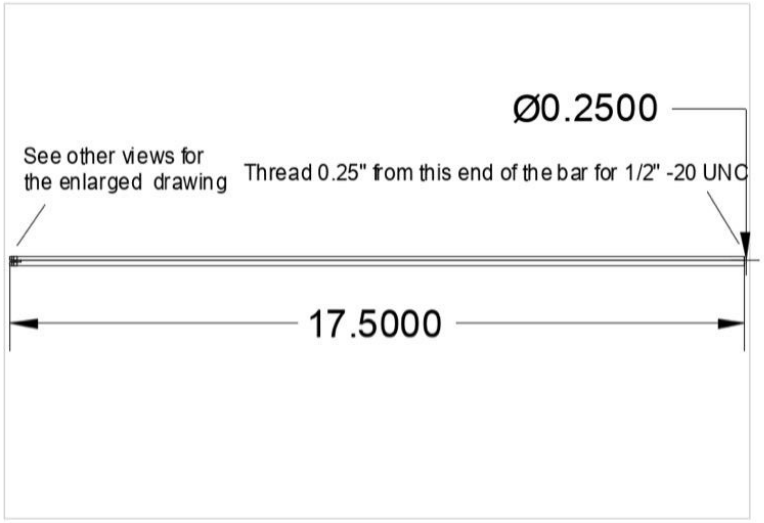

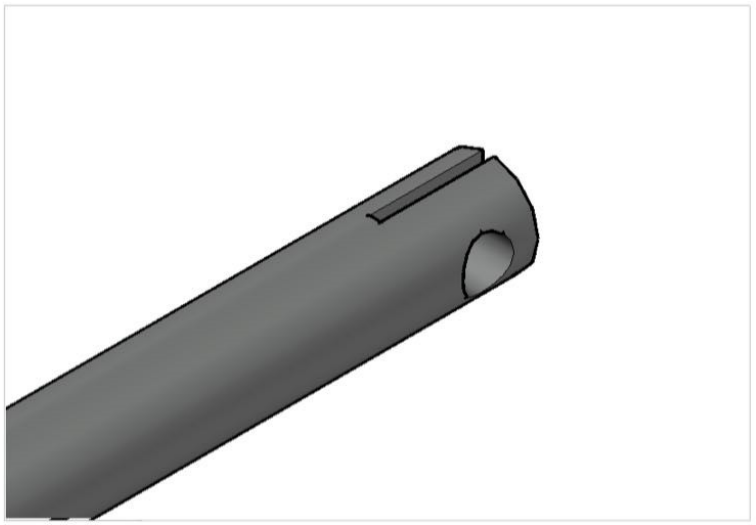

All dimensions in inches, the tolerance is ±0.0005. The material is 17-4 PH stainless steel. We need one of this,

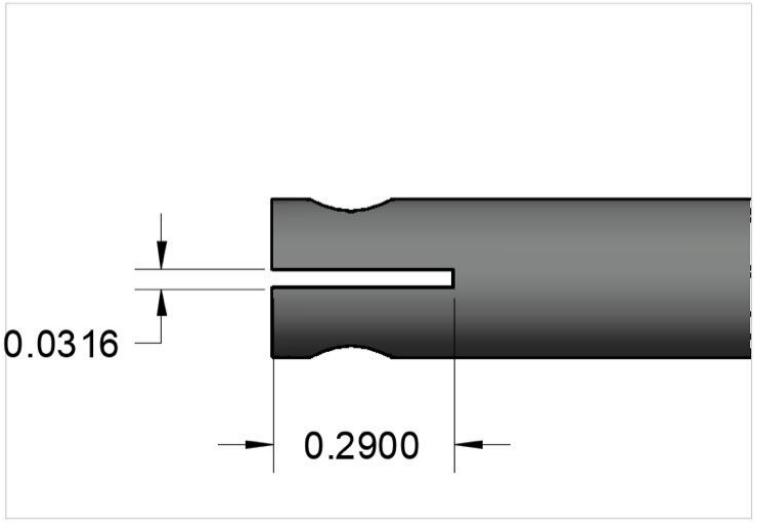

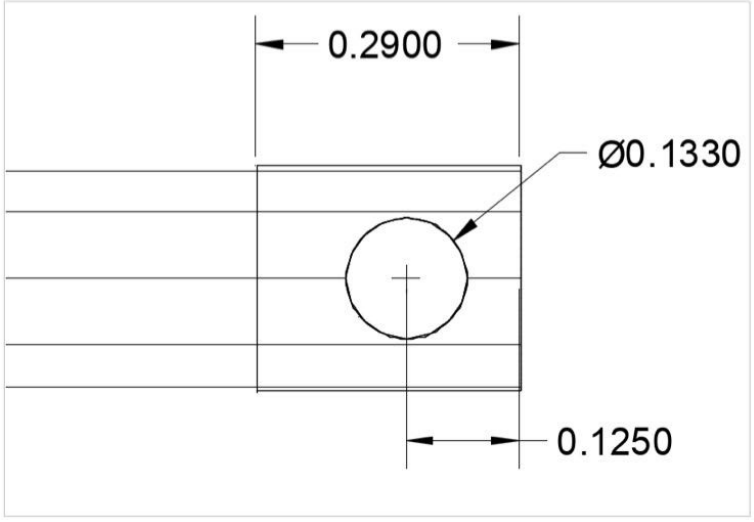

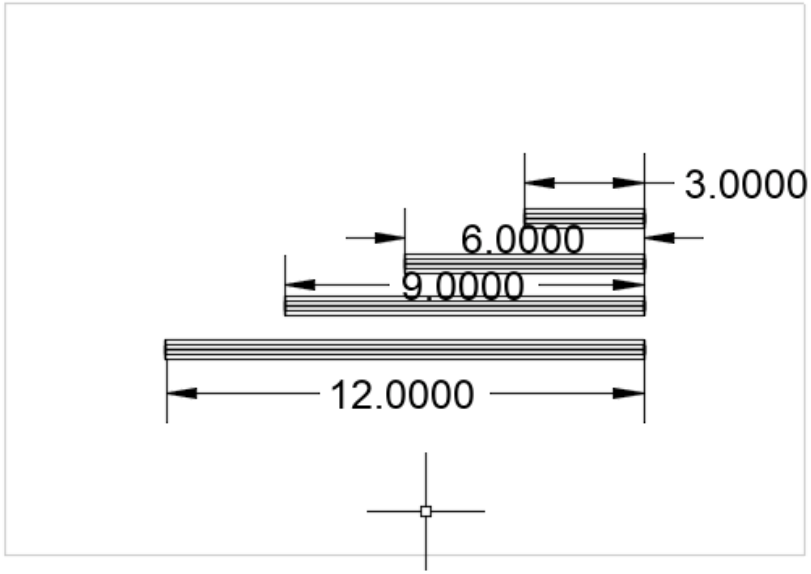

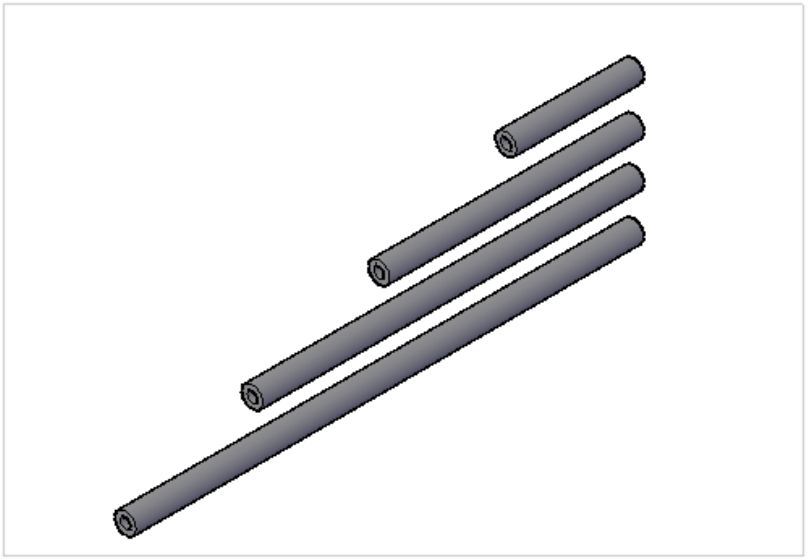

All dimensions in inches, the tolerance is ±0.0005. The material is Al 7075. We need one for each length.

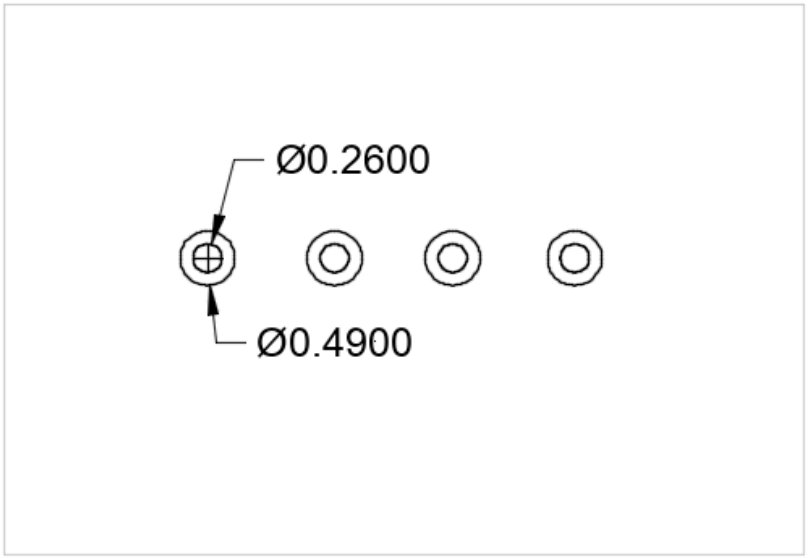

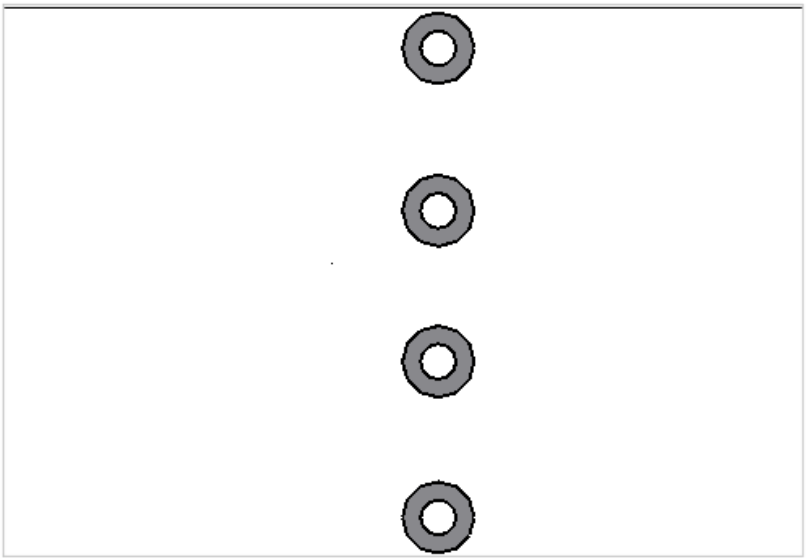

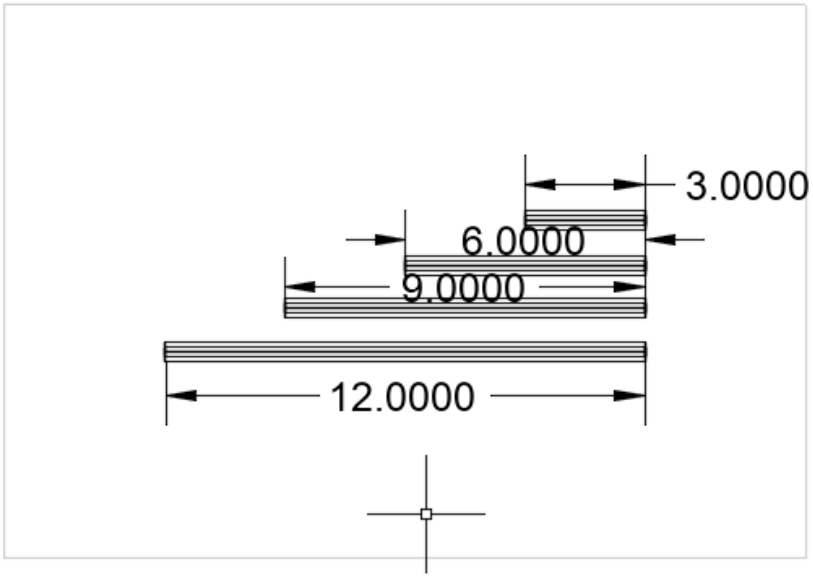

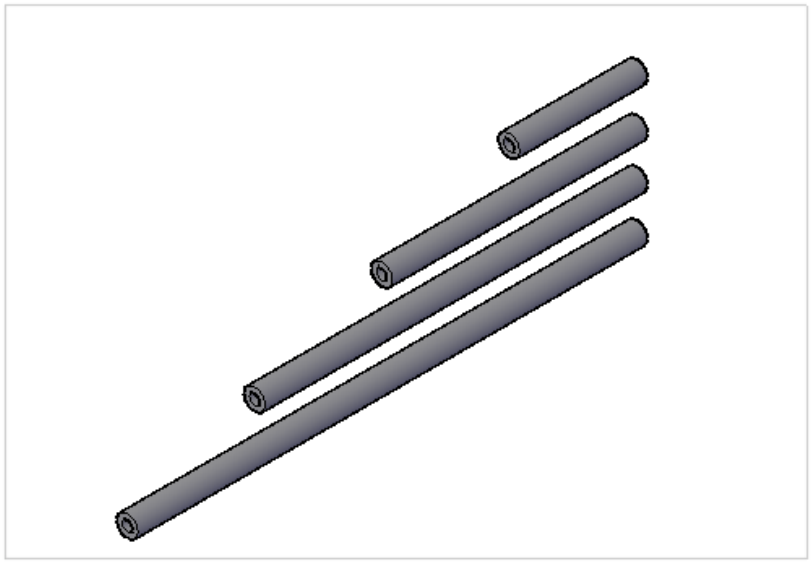

All dimensions in inches, the tolerance is ±0.0005. The material is Al 7075. We need one for each length.

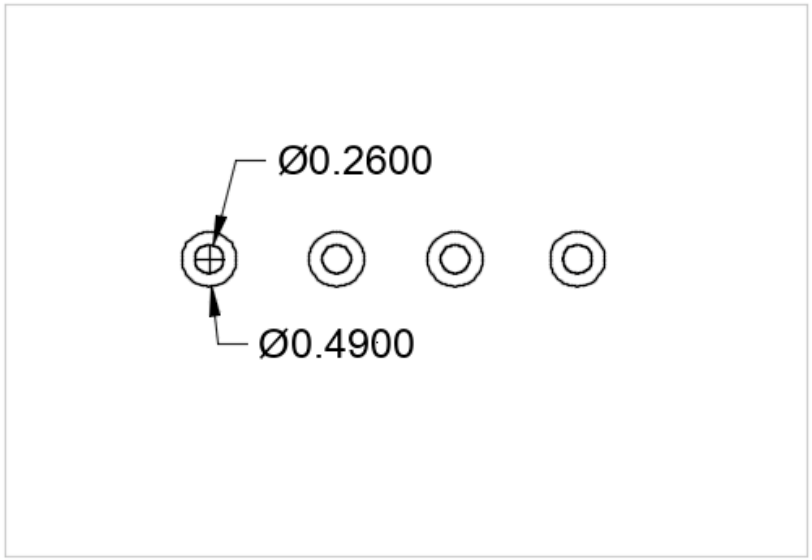

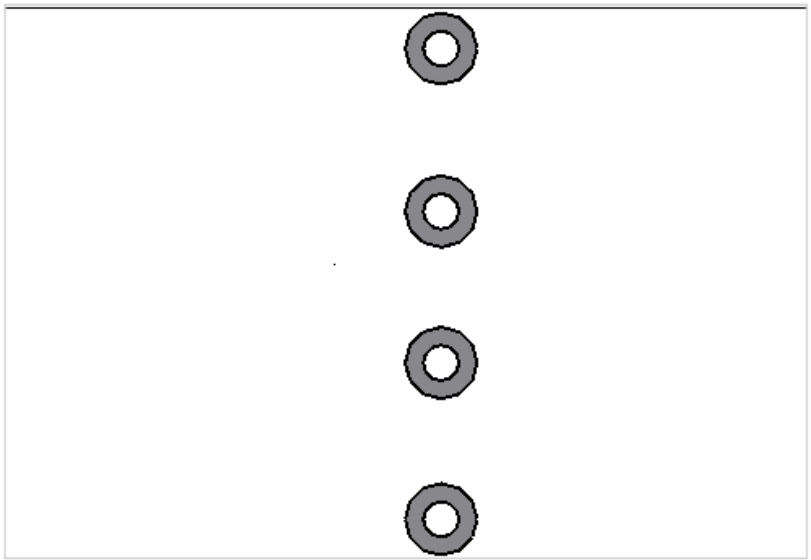

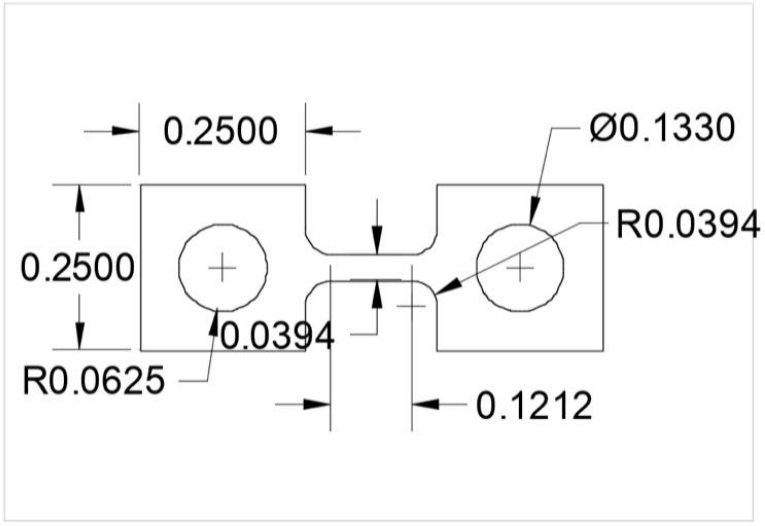

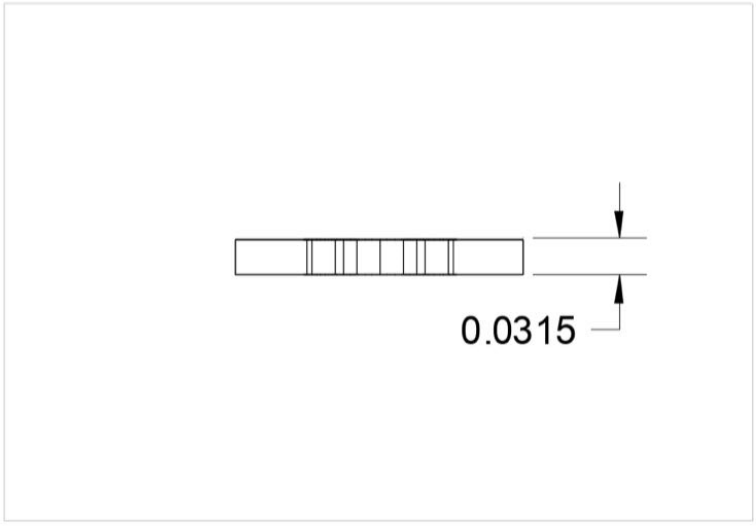

We need the code of this for wire EDM. All dimensions are in inches.

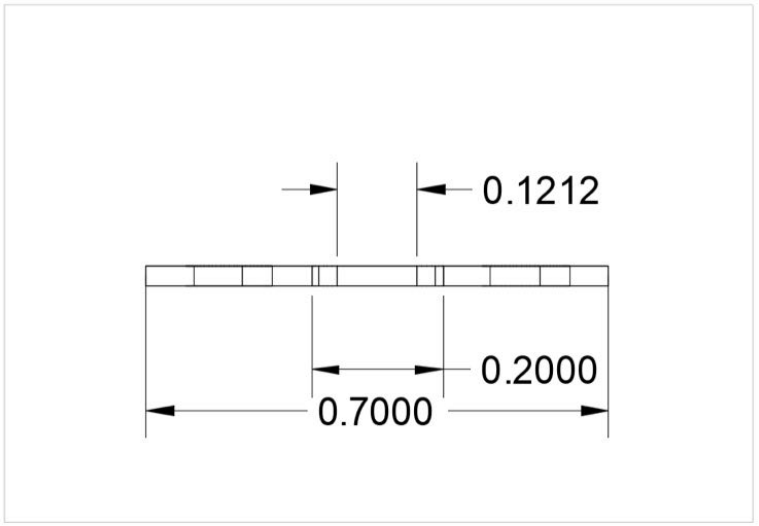

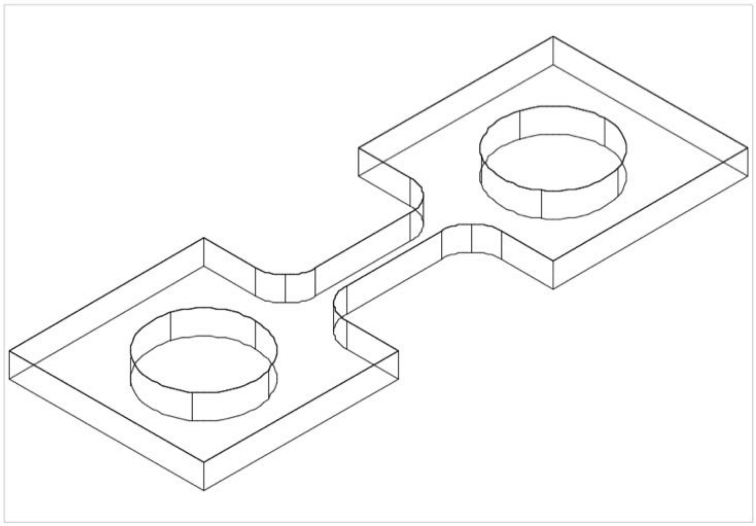

Resume

EDUCATION & AWARD **Ming Guan, Email: mguan3@jhu.edu**

Johns Hopkins University **Sept. 2017-Dec. 2020**
Master of Science and Engineering of Materials Science
Advisor: Todd Hufnagel

Stanford University **Sept. 2015-June. 2017**
Master of Science in Materials Science
GPA: 3.77/4.00

University of Science and Technology, Beijing **Sept. 2011-June. 2015**
Bachelor of Science in Materials Physics **Beijing, China**
GPA: 3.65/4.0 Major GPA: 3.7/4.0

Nankai middle school **Sept. 2008-June. 2011**

PUBLICATIONS:

1. X Liu, M Khan, W Liu, M Guan, P Jiang, W Cao*. "Synthesis of nanocrystalline Ga–TiO_2 powders by mild hydrothermal method and their visible light photoactivity". ***Ceramics International***, 2015, 41(2): 3075-3080.
2. Lei, T., Guan, M., Liu, J., Lin, H. C., Pfattner, R., Shaw, L., ... & Tok, J. B. H. (2017). Biocompatible and totally disintegrable semiconducting polymer for ultrathin and ultralightweight transient electronics. ***Proceedings of the National Academy of Sciences***, 114(20), 5107-5112.

RESEARCH EXPERIENCE

Todd Hufnagel research lab
Research Assistant and PhD student **Advisor: Prof. Todd Hufnagel**

- ✧ Dynamic deformation's effect on TRIP (transformation-induced plasticity) steel.
- ✧ Characterization (EBSD (Electron backscatter diffraction) and HEDM(high-energy diffraction microscopy)) and modeling of the influence of microstructure on deformation-induced martensite formation in TRIP steel.

Bao research lab
Volunteer Research Assistant **Advisor: Prof. Zhenan Bao**

Bio-decomposable transparent flexible polymer transistor

- ✧ Fabricated the fully bio-compatible and bio-decomposable transistor for the first time in this field.
- ✧ Demonstrated the high yield and reliability of new synthesized conjugated semiconducting DPP polymer on four different kinds of substrates (cellulose, silk, parylene and silicon dioxide).
- ✧ Proposed a new hydrolysis method to make a new cellulose substrate which is bio-decomposable.
- ✧ The transistor can work under relative low voltage(less than 5V) and high mobility(around 0.3 $cm^2/(v*s)$)
- ✧ A paper about it has been accepted by Proceedings of the National Academy of Sciences.

Carbon nanotube(CNT) sorting and deposition on circuit

- ✧ Used different kinds of imine bond recyclable polymers, centrifuge and ultra sonication to sort semiconducting CNT.
- ✧ Optimized the parameters to deposit CNT on circuit.
- ✧ The first time anyone in Prof. Zhenan Bao's group had made a flexible CNT logic transistor.

SKILL

- ✧ Be familiar with Split-Hopkins Bar and the high rate deformation experiment.
- ✧ Experience on 3D EBSD characterization on TRIP steel
- ✧ Experience on using HEDM characterization method to rebuild 3D plot of TRIP steel samples.